European Journal of Mechanics B/Fluids 30 (2011) 577–588

Contents lists available at SciVerse ScienceDirect

European Journal of Mechanics B/Fluids

journal homepage: www.elsevier.com/locate/ejmflu

Numerical wave breaking with macro-roughness

Alioune Nar Sambe [a,b,c], Damien Sous [a,*], Frédéric Golay [b], Philippe Fraunié [a], Richard Marcer [c]

[a] Laboratoire de Sondages Electromagntiques de l Environnement Terrestre, Université du Sud Toulon Var, BP 20132, 83957 La Garde Cedex, France

[b] Institut de Mathématiques de Toulon, Université du Sud Toulon Var, BP 20132, 83957 La Garde Cedex, France

[c] Principia, Zone Athelia 1, 215 voie Ariane,13705 La Ciotat Cedex, France

ARTICLE INFO

Article history:
Available online 10 March 2011

Keywords:
Wave breaking
Numerical simulations
Macro-roughness
Godunov
Interface

ABSTRACT

This paper reports on a numerical investigation of solitary wave breaking over a sloping bottom covered with macro-roughness elements. Wave breaking is simulated by solving Euler equations with a two phase incompressible flow model. The hyperbolic system of the conservation laws is solved with a finite volume discretization on an unstructured grid. An artificial compressibility approach allows the use of a fully explicit scheme for an efficient parallel implementation. The numerical model is based on a low Mach number preconditioning and a second order Riemann solver. Several test cases are performed to analyze the role played by macro-roughness on the breaking dynamics. The influence of the macro-roughness elements on the solitary long wave breaking is shown to depend on two dimensionless ratios D/A and H/A, where D, H and A are the separation distances between the macro-roughness elements, the height of the elements and the wave amplitude, respectively. Significant effects are observed for large values of D/A and H/A. The successive cycles of impact/splash-ups/rebounds are strongly impaired. Three-dimensional wave breaking simulations are presented, showing the robustness of the method for modeling complex wave-structure interactions.

1. Introduction

Carrying wind-induced or seismic energy from far–distant offshore areas, waves are a preponderant force in the near-shore zone and an essential parameter in beach morphodynamics and coastal structure engineering. As it propagates to the shore, the relatively well organized dynamics of offshore waves is transformed into a wide range of motions of different types and scales, see e.g. [1]. A major research effort, sustained over several decades, has brought great insight to our knowledge of the surf zone hydrodynamics, widely affected by breaking waves [2,3]. Wave breaking is generally the most dominant phenomenon in the near-shore energy budget. It therefore appears that improving our predicting capacities of wave breaking is of primary importance. In particular, impact kinematics and run up on structures and beaches are drastically important in the case of hazardous events like storms, surges and tsunamis. Coastal communities clearly benefit from the protection offered by natural (coral reefs, rocks, mangroves) or engineered (buildings, concrete blocks, jetties) obstacles. Indeed, research works have recently been engaged to quantify the effectiveness of such barriers in mitigating coastal impacts (e.g. [4]).

In that context, the present study aims at numerically analyzing the wave breaking over a sloping bottom covered by macro-roughness. By contrast to skin friction which only acts on the bottom shear stress, the presence of macro-roughness modifies the whole flow field, i.e. by accelerating and decelerating the flow up to the free surface. Our primary objective is thus to understand how the roughness elements will affect the breaking dynamics.

Different numerical approaches are generally used for modeling wave transformation reaching the shore. On one hand, models based on Boussinesq equations are fast but unable to compute wave breaking [5,6]. On the other hand, the classical full Navier–Stokes solvers allow relevant and accurate results all along the wave shoaling and breaking processes [7–11]. However, the wave breaking process is a very complex phenomena, involving intense turbulence with a wide variety of length-scale and strong mixing between air and water. The detailed description of the whole physics including three-dimensional viscous and turbulent dissipation and surface tension effects often leads to unacceptable computation time on standard computers, see e.g. [12]. Similarly, it has been shown that SPH methods on 3D problems lead to prohibitive computation times [13].

As the present study aims at finding an efficient compromise between computation costs and physical relevancy, an alternative numerical method is proposed. It is based on a fast three-dimensional two phase flow solver, with a finite volume discretization on unstructured grids with subdomains decomposition

* Corresponding author.
E-mail address: sous@univ-tln.fr (D. Sous).

0997-7546/$ – see front matter © 2011 Elsevier Masson SAS. All rights reserved.
doi:10.1016/j.euromechflu.2011.03.002

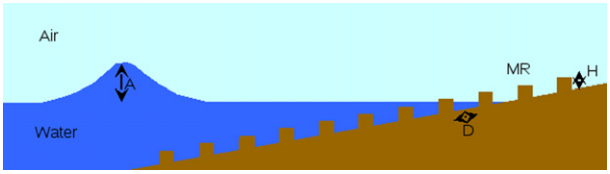

Fig. 1. Wave breaking: solitary wave and sloping beach covered with macro-roughness elements.

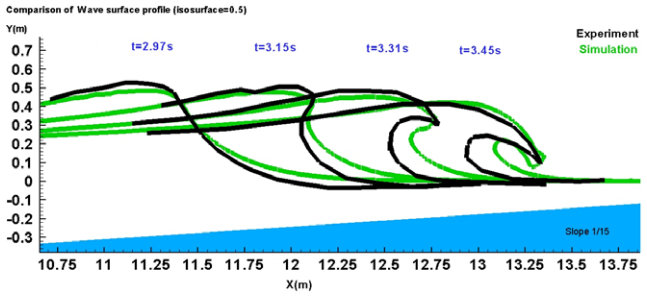

Fig. 2. Validation case: comparison with the experimental study of Li and Raichlen [28] on the basis of the Grilli's wave breaking case [29].

allowing an efficient parallel implementation. For the present work, the model basis has been validated on experimental [14] and numerical test cases with convincing numerical performances and computational time, see [15]. The method has next been improved by the selection of an isothermal model and relevant numerical techniques in [16]. Both viscous and turbulent dissipations are neglected in order to avoid the discretization of the Laplacian operator and allow to use a fast hyperbolic solver. Equations of conservation are solved in a single domain by introducing a state equation depending on the volume fraction of water and air [17,18]. The equation of state of our average mixed model is artificial, but numerically relevant. The volume fraction is thus transported without tracking or reconstructing the interface, as in VOF methods (see e.g. [19]). Similar approaches have been successfully compared to classical fully NS models on dam break and wave breaking problems [11] and also been used to simulate violent aerated flows [20]. It should be emphasized that energy dissipation is not taken into account. The model applicability should be strictly limited to the early stages of the breaking process. For longer times, bottom friction and turbulence have a major effect on the breaking wave dynamics. As the model does not include this dissipation, it would be meaningless to evaluate late features from the present computation, such as run up height. However, in the selected test cases, the wave breaking is a violent plunging breaking, the splash-up cycles occur in a very shallow water layer or even directly rebound on the macro-roughness elements. It is then assumed that the breaking dynamics is dominated by impacts, pressure shocks and large coherent structures rather than by bottom friction or a well-established turbulent energy cascade.

The present study aims to pursue the work engaged in [21] on the numerical modeling of wave-breaking in presence of

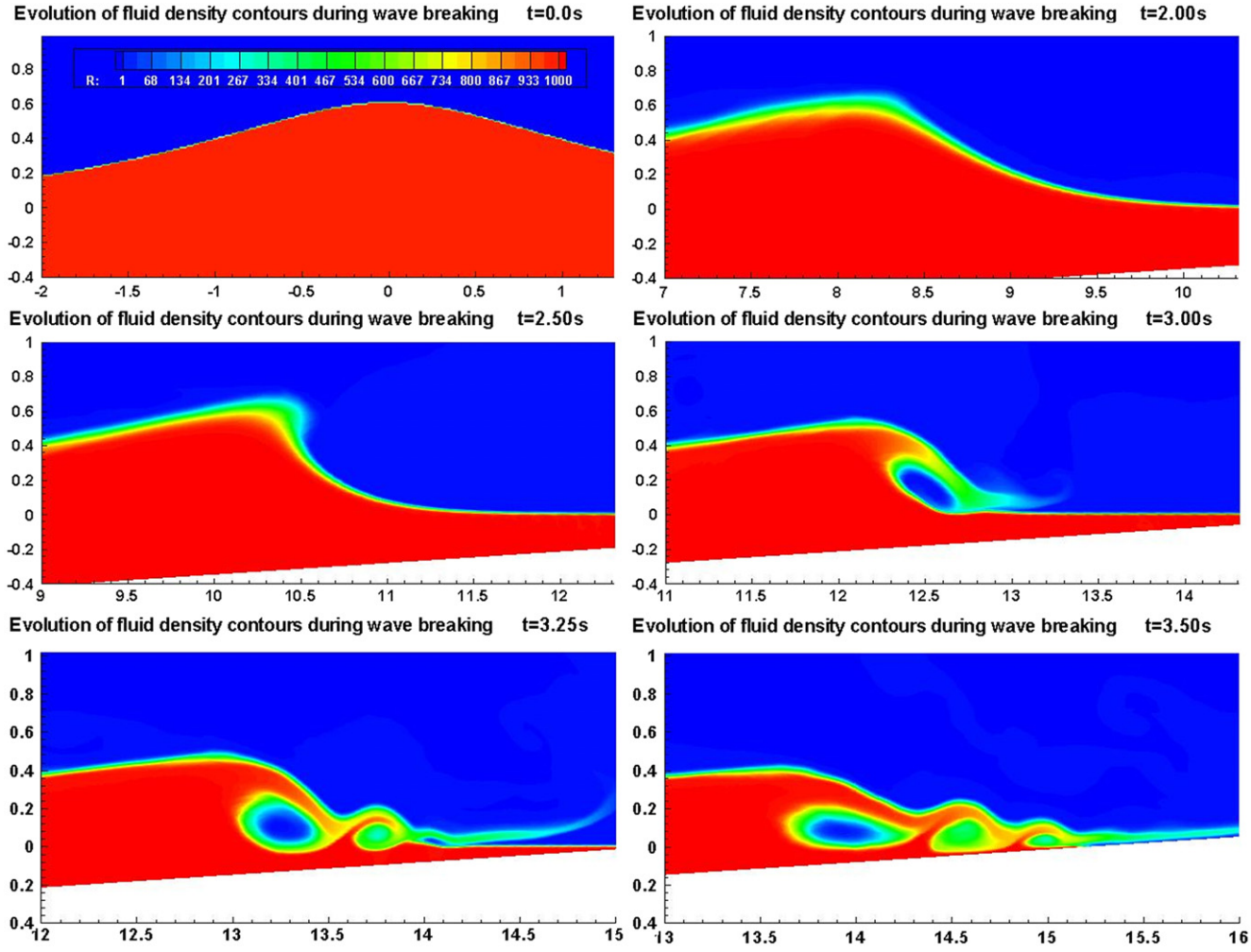

Fig. 3. Evolution of the fluid density contours during the solitary wave breaking process for case H00D00 (flat sloping bottom) at $t = 0$, 2, 2.5, 3, 3.25 and 3.5 s.

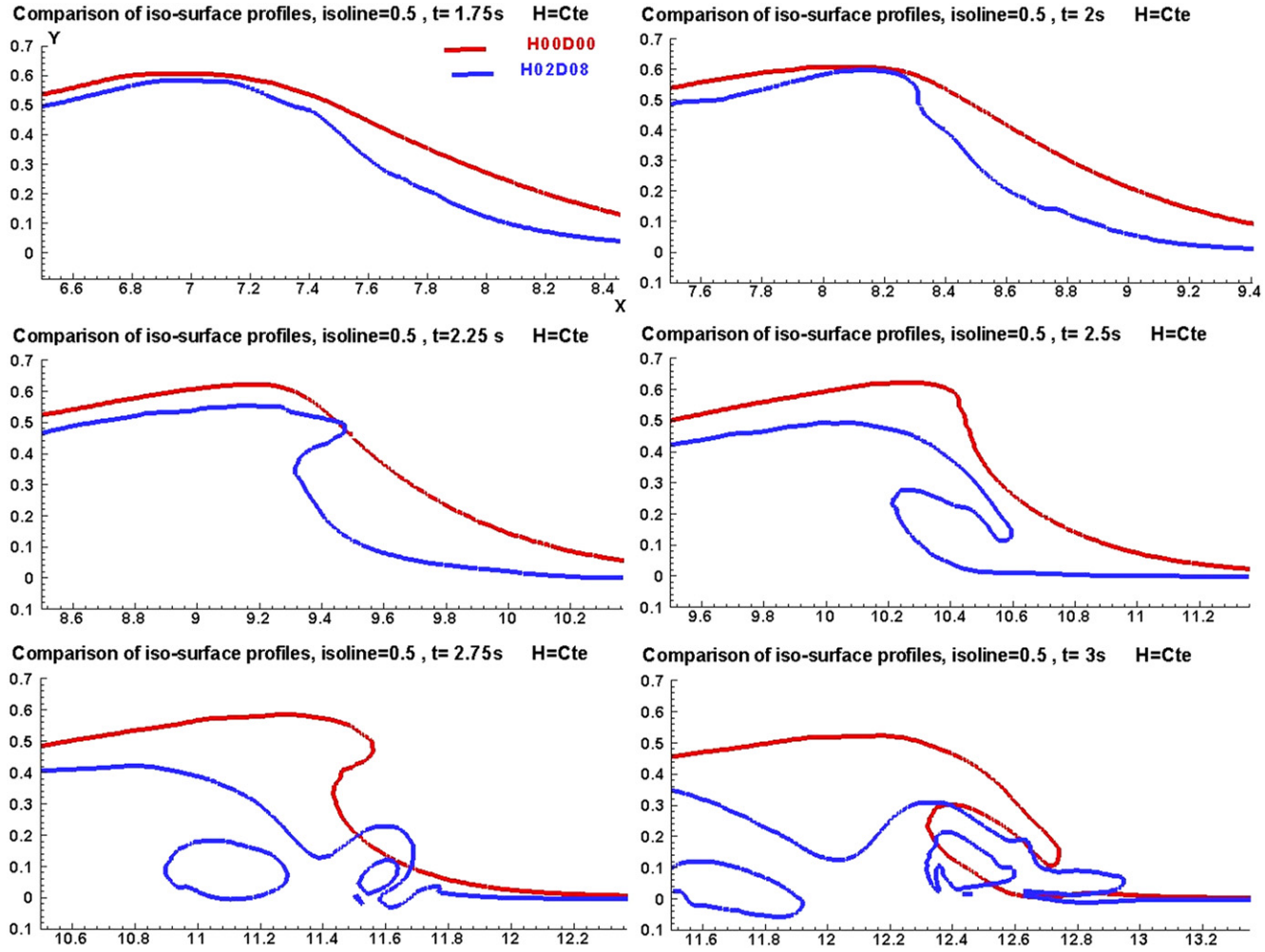

Fig. 4. Compared evolution of the free surface profile during the solitary wave breaking process for cases H00D00 (flat sloping bottom) and H02D08 (rough sloping bottom), at $t = 1.75$, 2, 2.25, 2.5, 2.75 and 3 s.

macro-roughness. The paper is organized as follows. The first and second parts describe mathematical model and numerical methods, respectively. The third section presents the computational domain used for wave breaking test cases. Results and analysis are proposed in the fourth section while the last part is dedicated to conclusions and prospects.

2. Model and method

2.1. Mathematical formulation

An Eulerian 3D, compressible, inviscid two phase flow model is used, leading to an hyperbolic system of conservation laws for mass and momentum. An optimized artificial compressibility approach at low Mach number allows a fully explicit scheme. The computed variables, the density ρ, the velocity $\vec{U}$, the pressure p and the fraction of water ϕ depend on spatial position (x, y, z) and time t. The volume fraction satisfies $0 \leq \phi \leq 1$, with $\phi = 1$ in the water and $\phi = 0$ in the air. Considering the gravity $\vec{g}$, neglecting viscous effects and superficial tension, but introducing artificial compressible effects, we consider the following 3D Euler equations in the isothermal case:

$$\frac{\partial \rho}{\partial t} + \mathrm{div}(\rho \vec{U}) = 0 \tag{1}$$

$$\frac{\partial \rho \vec{U}}{\partial t} + \mathrm{div}(\rho \vec{U} \otimes \vec{U} + p) = \rho \vec{g} \tag{2}$$

$$\frac{\partial \phi}{\partial t} + \vec{U}.\nabla \phi = 0 \tag{3}$$

$$p = p(\rho, \phi). \tag{4}$$

In this model, the pressure depends on the volume fraction which allows to distinguish between the liquid (water) and the gas (air). An "Equation Of State" (EOS) has to be adequately chosen. Let $c(x, y, z, t)$ denote the sound speed. It is usually admitted in physics that a flow is incompressible if the Mach number is lower than 1/10. Here, the real (physical) Mach number is generally much smaller, of the order of 1/400–1/1600. With an explicit finite volume solver, the time step Δt is thus restricted by the CFL condition:

$$\Delta t = \alpha \frac{h}{\|\vec{U}\| + c} \tag{5}$$

where α is the CFL number and h the space step (e.g. the volume over the surface of the cell). Furthermore, it is known that numerical accuracy decreases due to the low Mach number of the flow. For those two reasons, an artificial pressure law has been chosen in which the sound speed is approximately fixed to 20 m/s. A simple but efficient choice of EOS is the isothermal gas EOS [16] that reads

$$p = c_0^2(\rho - (\phi \rho_A + (\phi - 1)\rho_W)) + p_0 \tag{6}$$

where ρ_A denotes the air density, ρ_w the water density, c_0 the artificial sound speed and p_0 a parameter.

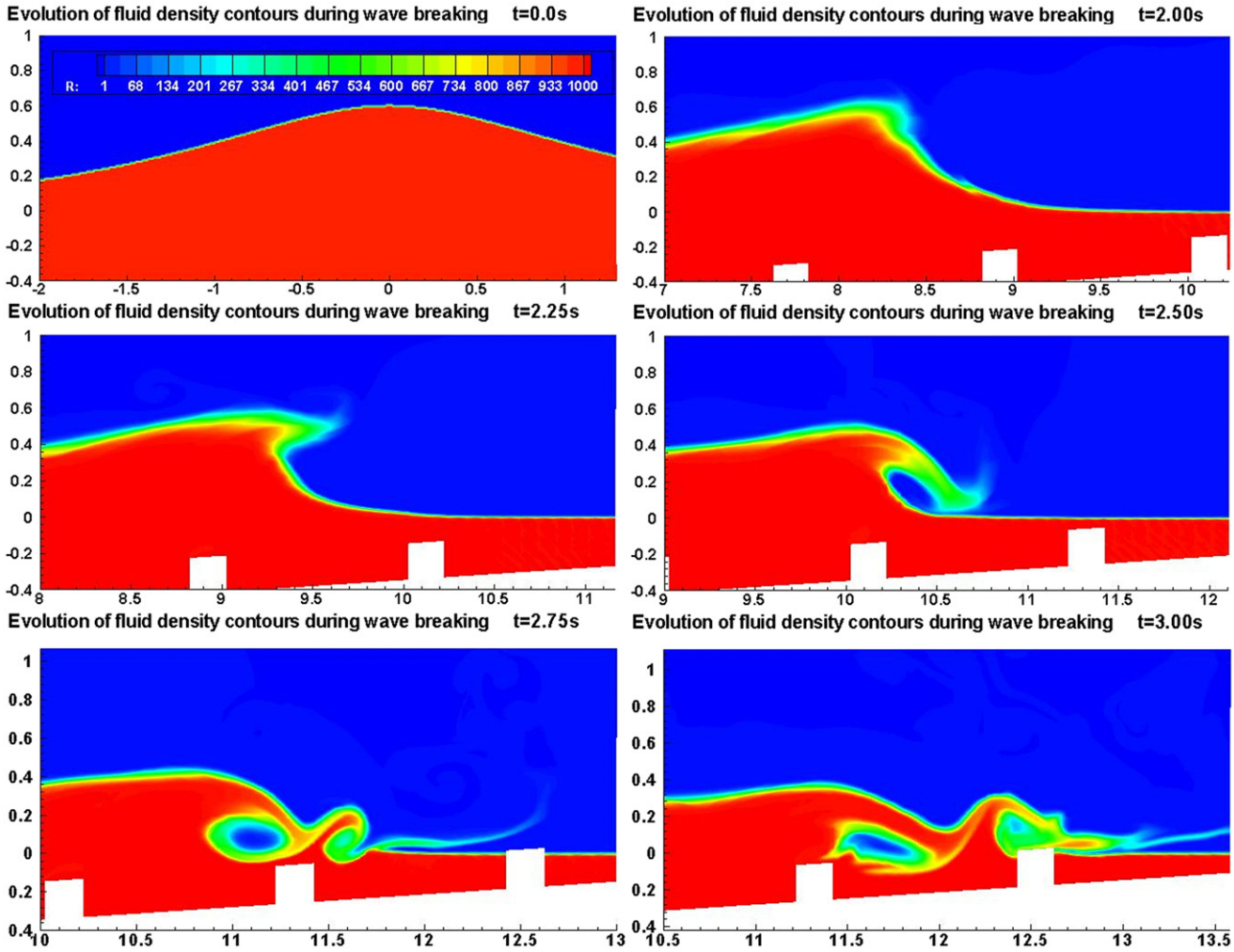

Fig. 5. Evolution of the fluid density contours during the solitary wave breaking process for case H02D08 (rough sloping bottom) at $t = 0, 2, 2.25, 2.5, 2.75$ and 3 s.

Remark 1. This numerical model was previously based on a stiffened gas EOS, involving an energy conservation equation [16]. Numerical results showed that, in the case of a solitary wave breaking, the isothermal EOS is physically and numerically relevant. It allows a significant CPU time saving by avoiding penalizing CFL conditions due to fast pressure oscillations.

Remark 2. In the present computations, the flow velocity will typically be of the order of 1 m/s. An optimized value of artificial sound speed $c_0 = 20$ m/s has been chosen to limit, on one hand, the compressibility effects and, on the other hand, the numerical diffusion and the CFL constrain.

Remark 3. Our pressure law has no physical meaning inside the mixture zone $0 < \phi < 1$ induced by numerical diffusion effects. The air–water mixing is a complex phenomena. The numerical diffusion and the thickening of the interface should never be assimilated as a relevant tracer of the mixing between air and water. The next step of the model development, which is already engaged, is to implement an efficient interface sharpening method to minimize the spurious free surface diffusion [22]. Recent studies have been engaged to provide a more physically relevant description of the mixed zone [23]. However, further developments and comparisons with experiments must be performed before the implementation of such tool in the present code.

2.2. Numerical method

A finite volume approximation with an exact Riemann solver (Godunov scheme) is used. To avoid pressure oscillations of the Godunov scheme occurring in multi-fluid cases, the Abgrall method [24] preserves from the occurrence of a moving contact discontinuity. This condition leads to a non-conservative discretization (Eq. (3)). To use a fully conservative scheme, it would be necessary to consider a pressure law imposing pressure equilibrium of the two components [17,25]. In order to get the interface with accuracy, a second order approximation in time and space (MUSCL) is used. Time discretization is explicit (midpoint Euler) and space discretization is based on slope reconstruction. In two-fluid problems, it is often necessary to perform an additional slope limitation at the interface between the two fluids. For these reasons, the Barth limiter [26], which is faster and gives quite good results with competitive computing time in spite of a small distortion of the interface, has been selected. Details concerning the numerical methods can be found in [16]. As explained in the introduction, the effects of molecular and turbulent viscosities on the breaking process are here neglected.

3. Wave breaking simulations

3.1. Computational domain

Several numerical simulations of solitary wave breaking over a sloping bottom have been performed. The computational domain

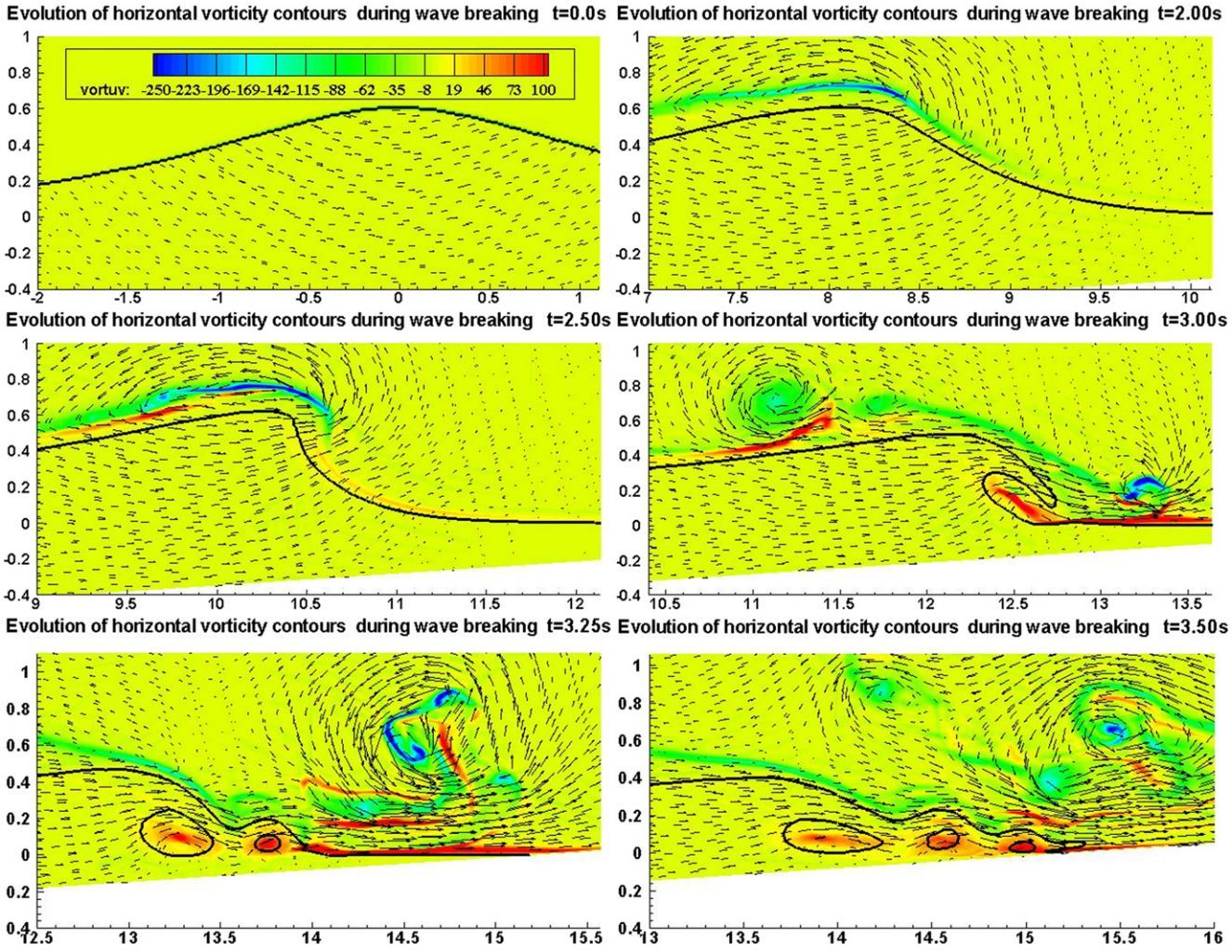

Fig. 6. Evolution of the vorticity fields and velocity vectors during the solitary wave breaking process for case H00D00 (flat sloping bottom) at $t = 0$, 2, 2.5, 3, 3.25 and 3.5 s.

is 25 m long and 2.5 m high (Fig. 1). The bottom is flat for $x < 5.225$ m and sloping for $x > 5.225$ m following $B(x, y) = (x - 5.225)/15$. The initial condition is a stable solitary wave computed with the Tanaka method [27], which is an incompressible potential solution of the Euler equations. The crest of the solitary wave is at $A = 0.6$ m over the still water level, except for the Li's case where $A = 0.45$ m. A mirror condition is imposed on the lateral sides. The Courant–Friedrichs–Levy number is fixed to 0.9. In order to reduce computation time, a parallel version of the finite volume scheme is implemented, using the library Message Passing Interface (MPI). A regular mesh, made of hexahedra, is split into 12 sub-domains. Each sub-domain is devoted to one process on the cluster (CPUs Itanium II at 1.5 GHz). The 2D simulations (about 1 million of cells, 2827×375) require 2 days CPU time and the 3D simulations (about 9.5 million of cells, $1052 \times 180 \times 50$) require about 12 days.

3.2. Description of the test cases

An ensemble of seven numerical simulations has been carried out, see Table 1. The first one, referred to as the Li's case, is dedicated to the validation with the experimental results of Li and Raichlen [28].

The six others, called H00D00, H01D04, H02D04, H03D04, H02D08 and H02D12, are performed to understand how the presence of macro-roughness (MR hereinafter) can affect the wave breaking process. Recall here that, by MR elements, we refer to bed forms which extend far above the equivalent boundary layer on flat bottom and are expected to produce accelerations and decelerations in the flow field all the way to the free surface. The reference case, H00D00, is the flat sloping bottom presented in [21]. Five rough bottom cases have then been simulated to analyze the breaking dynamics modifications and to understand the influence of MR elements physical parameters. The height and separation distance of the rectangular 0.2 m width elements are presented in Table 1.

Table 1
Summary of the test cases.

Case name	A (m)	H (m)	D (m)
Li's case	0.45	Flat	Flat
H00D00	0.6	Flat	Flat
H01D04	0.6	0.1	0.4
H02D04	0.6	0.2	0.4
H03D04	0.6	0.3	0.4
H02D08	0.6	0.2	0.8
H02D12	0.6	0.2	1.2

3.3. Validation case on a flat sloping bottom

The validation of the numerical results from the wave propagation until the jet impact, including shoaling and overturning processes, is based on the wave breaking study on a flat sloping bottom first proposed by Grilli et al. [29]. They used a two-dimensional fully nonlinear potential flow model to calculate

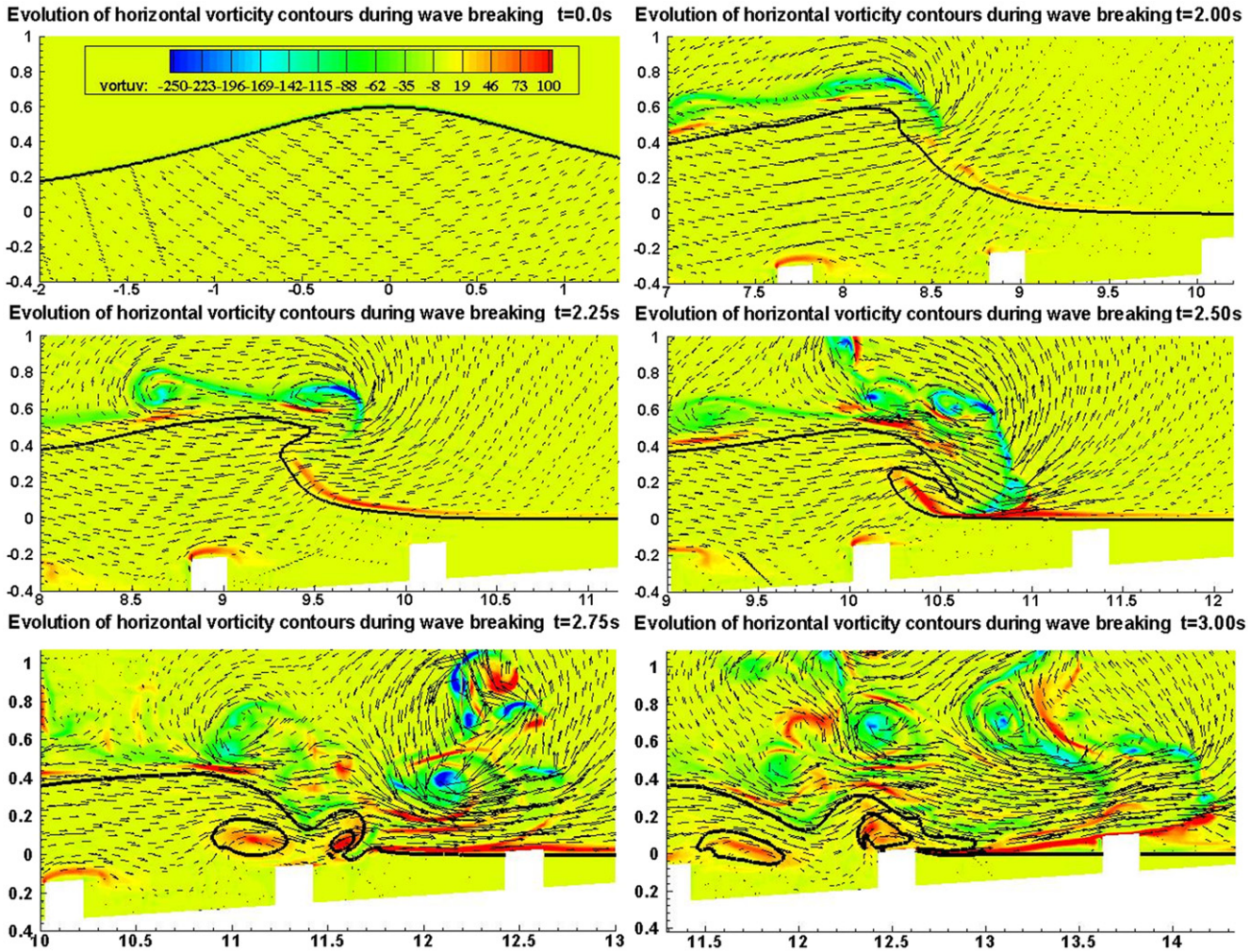

Fig. 7. Evolution of the vorticity fields and velocity vectors during the solitary wave breaking process for case H02D08 (rough sloping bottom) at $t = 0$, 2, 2.25, 2.5, 2.75 and 3 s.

various characteristics of solitary waves propagating within a constant depth and then shoaling and breaking on several different slopes. This case has then been experimentally studied by Li and Raichlen [28] and is referred here as the Li's case. Fig. 2 shows a comparison of the experimental and numerical free surface profiles at times $t = 2.97$, 3.15, 3.31 and 3.45 s. One can note the good agreement between experiments and numerical predictions. The wave steepening, the overturning dynamics and the impact position are well predicted. Some discrepancies can be observed in the wave shape in particular just before the impact ($t = 3.31$ and 3.45 s), but the general agreement is very satisfactory regarding our fast numerical model.

For the overall breaking dynamics after the impact, a comparison can be done with existing numerical studies, see e.g. [30]. The restrictions exposed in the introductive section are recalled here: as turbulence and viscous effects are not taken into account, the model applicability is limited to the first stages of the breaking process during which it can be assumed that breaking dynamics is dominated by impacts, rebounds and large scale vortical structures. The results presented here are therefore restricted to short times ($t < 3.5$ s). The breaking process is described in Fig. 3 for the flat sloping bottom case H00D00, which is used hereinafter as the reference case for the study of macro-roughness influence (see Table 1). Fig. 3 presents contours of fluid density at successive stages of the breaking process.

The wave first propagates without deformation. About $t = 2$ s, the shoaling process starts and the wave progressively steepens and becomes more and more asymmetric during its propagation. After $t = 2.5$ s, the front face of the crest becomes nearly vertical and the breaking process starts, converting potential energy into kinetic energy. A fluid jet is ejected from the wave crest, and free falls under the action of gravity. The jet then impacts on the flat part of the free surface, inducing a characteristic overturning motion. The splash-up process develops when the jet rebounds on the free surface and probably partly pushes up the underlying water previously undisturbed. The overturning motion then repeats twice, each successive cycle of jet ejection/impact/splash-up being weaker than the previous one. Gas pockets are trapped into the vortices cores. The comprehensive validation for this complex case will necessarily require 3D high resolution experiments. However, these numerical results can be qualitatively compared with existing numerical study [30] or experiments [31]. This confirms the interest of our approach in which, for the selected cases, the early stages of wave breaking can be adequately represented even if turbulence and friction effects are neglected.

3.4. Influence of the macro-roughness elements

3.4.1. Comparison between flat and rough cases

To understand the overall effect of MR, let us compare first the reference flat sloping bottom case H00D00 with the intermediate rough case H02D08. The compared evolution of the free surface for both cases during the breaking process is presented in Fig. 4.

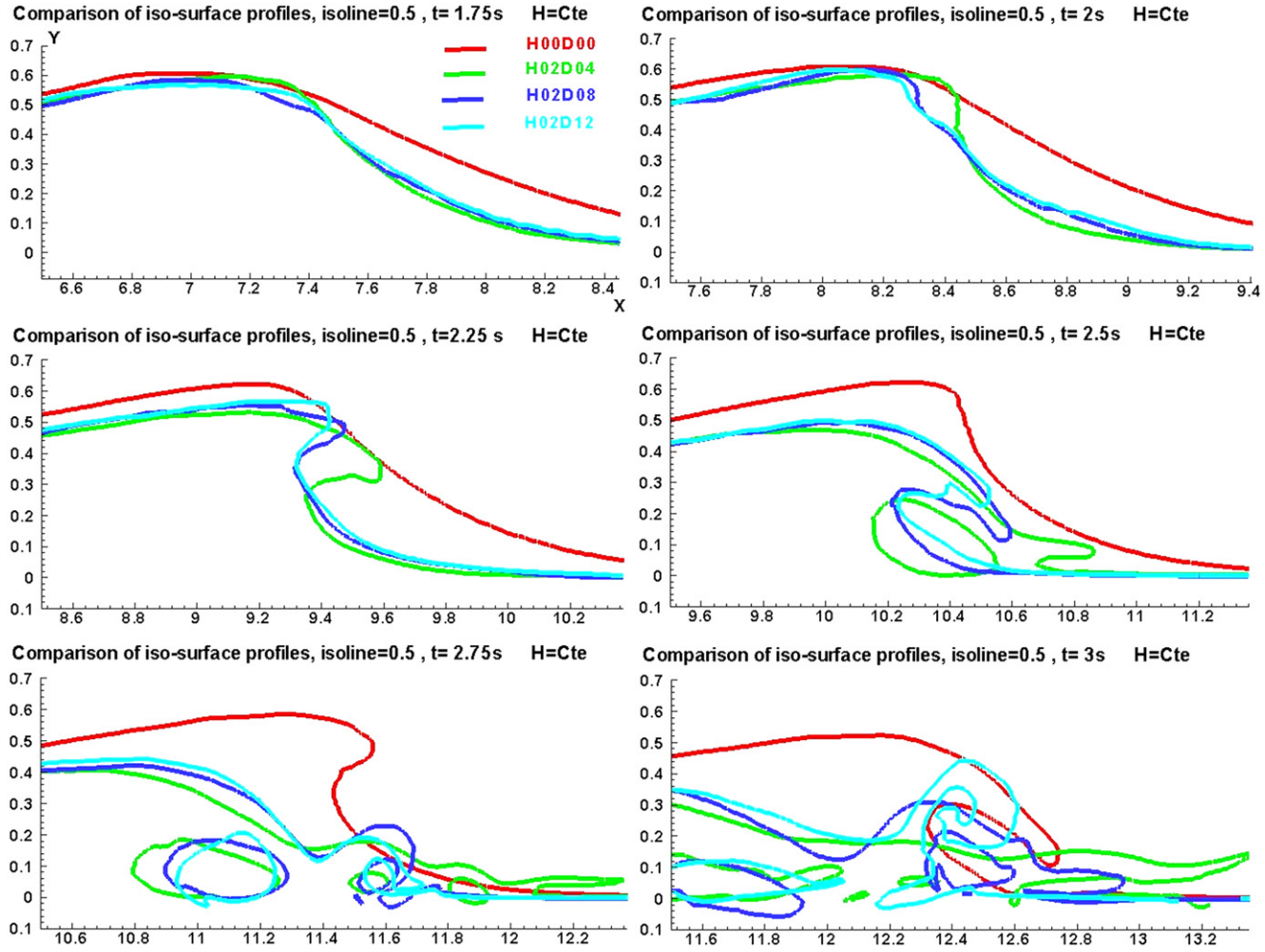

Fig. 8. Influence of the separation distance between the macro-roughness elements on the solitary wave breaking—Compared evolution of the free surface profile for cases H00D00, H02D04, H02D08, H02D12.

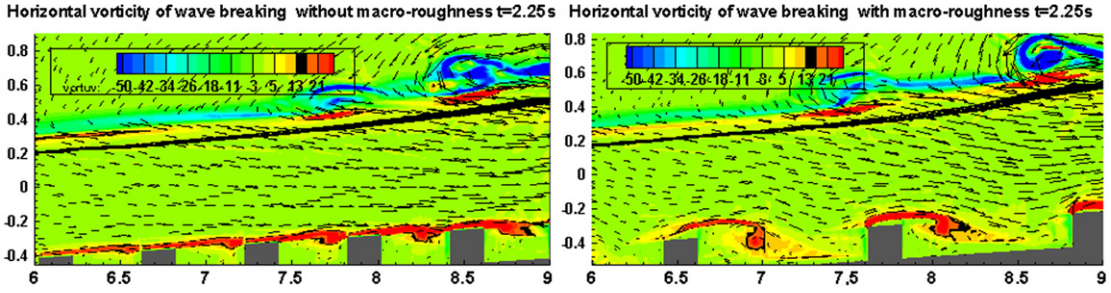

Fig. 9. Compared vorticity fields at $t = 2.25$ s for cases H02D04 (left) and H02D08.

One can note first that the presence of MR elements affects the free surface profile during the shoaling process, i.e. even before the wave breaking. The free surface is perturbed by small oscillations of few centimeters in amplitude and around 0.5 m in wave length. The origin of such humps will be explained later. At $t = 2.5$ s, the jet is close to the impact for the MR case whereas the reference case has not even reached the critical breaking slope. It is clear that both shoaling and wave breaking processes are accelerated by the MR and the breaking point appears earlier in time and space. Until the impact occurs, the wave overturning is very similar for both cases, see H00D00/$t = 3$ s and H02D08/$t = 2.5$ s. Once the ejected water mass impacts the free surface previously at rest, the breaking dynamics is strongly affected by the presence of MR elements. It is clearly seen in Figs. 3 and 5 which compares the evolution of fluid density contours for both cases.

MR induce an earlier wave breaking, which leads to a jet impact in deeper water. It can be seen by comparing Figs. 6 and 7 that a layer presenting of deficit of momentum develops between the roughness elements due to the form drag. This is balanced by a momentum excess confined in the upper part of the wave that accelerates the wave crest and thus induces an earlier breaking for the rough case. As the wave breaks lower on the slope, the shoaling process is interrupted earlier than in the flat reference case. This explains the wave amplitude difference between rough and flat cases illustrated in Fig. 4. Moreover, as the wave still propagates during the breaking process, the

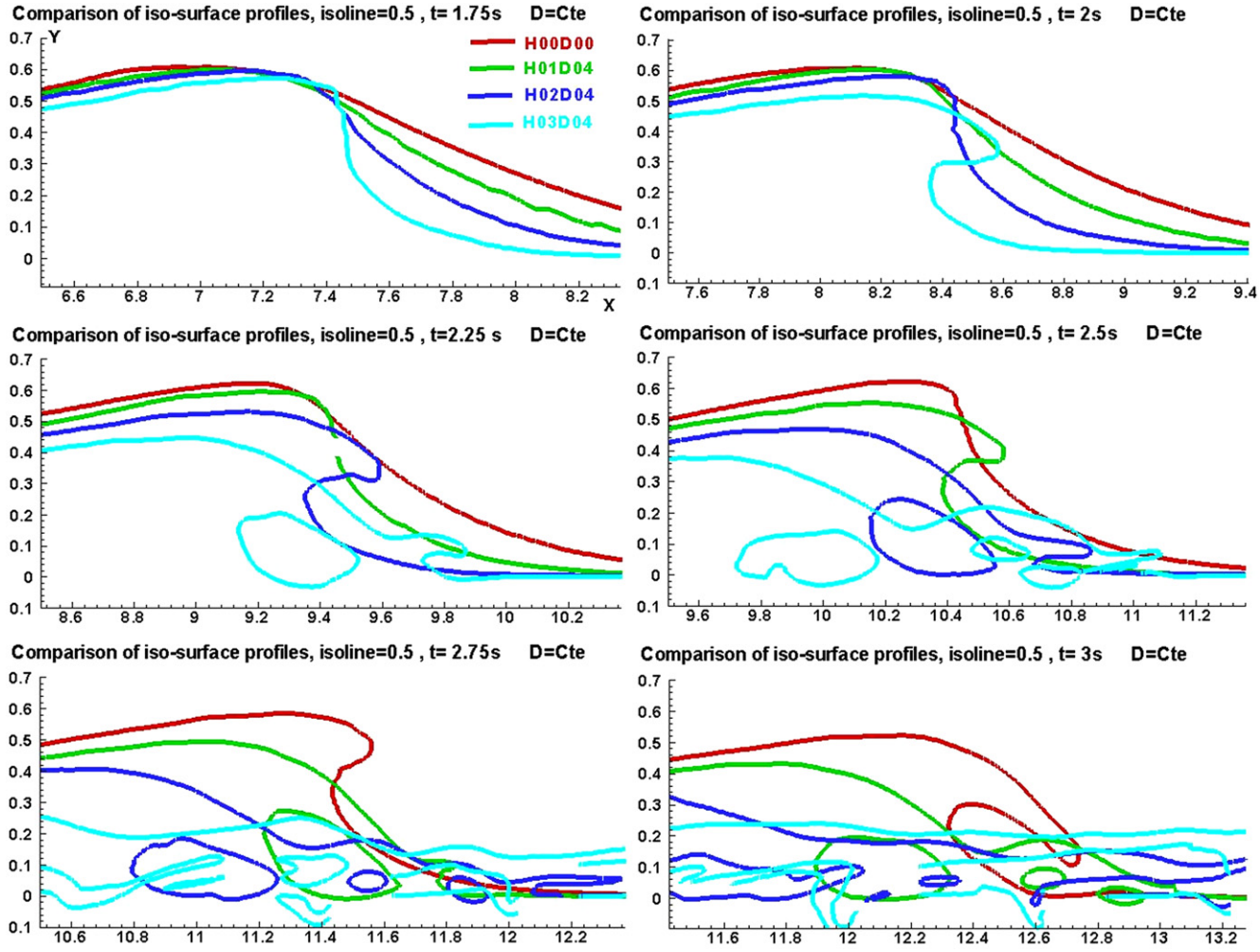

Fig. 10. Influence of the height of the macro-roughness elements on the solitary wave breaking—Compared evolution of the free surface profile for cases H00D00, H01D04, H02D04, H03D04.

well-know overturning and successive cycles of jet ejection / splash-up / rebounds are strongly impaired by the presence of MR. The splash-up dynamics depends on the MR location on the slope. They can be either reinforced when encountering the roughness elements (Fig. 5, $t = 3$ s) or possibly weakened by the impact in deeper water.

The origin of free surface humps is clarified by comparing the vorticity fields in Figs. 6 and 7, for flat and rough cases respectively. Looking carefully at the vicinity of the MR elements for the rough case (Figs. 6 and 7, $t = 2$ s and after), the presence of vorticity patches around each element related to the presence of a sheared zone can be identified. This deformation of the fluid streamlines affects the flow all the way up to the free surface and eventually affects the structure of the sheared layer over the free surface, as shown for instance in Figs. 6 and 7 for $t = 2$ s. This explains the free surface disturbances noted for the rough case in Fig. 4. For $t > 2$ s the vorticity is much more intense and irregular, in particular in the air phase in the vicinity of the water jet. It should be noted here that the quite turbulent aspect of fluid flow in the air has to be considered with caution. Several tests have been performed which showed that decreasing the height of the domain enhances the turbulent activity in the air. The vertical extension of the computation domain has then been chosen in order to be a satisfactory compromise between CPU time and physical relevancy. However this spurious effect is limited to the air flow, which can possibly increase the interface diffusion, but no significant influence on the water phase dynamics has been observed during the wave breaking process.

Hence, the influence of the presence of MR elements for the presented case H02D08 can be summarized as follows: (i) an earlier and deeper breaking point, (ii) significant streamlines deformations around the MR elements all the way to the free surface, (iii) a strong disturbance of the successive cycles of impact/splash-ups/rebounds and (iv) an expected smaller extent of run up on the slope.

3.4.2. Parametric study

Parametric study over the six cases presented in Table 1 has showed the important role played by the separation distance D between the MR elements. This is demonstrated by the comparison of the free surface profiles shown in Fig. 8. One can note that, first, the location of the breaking point as well as the time for the wave overturning and the jet impact are only weakly affected by a varying D. The comparison of free surface profiles during the wave shoaling and overturning shows that free surface disturbances observed previously and attributed to the modifications of the flow topology by MR are enhanced for a large D (case *H02D12*) and damped for a small D (case *H02D04*). A stronger influence of D is observed on later stages of the wave breaking. For a small D (case *H02D04*), the overall dynamics is quite similar to the flat case and the successive splash-up cycles are well defined at least for $t < 3.5$ s. For a large D, the late breaking stages are strongly

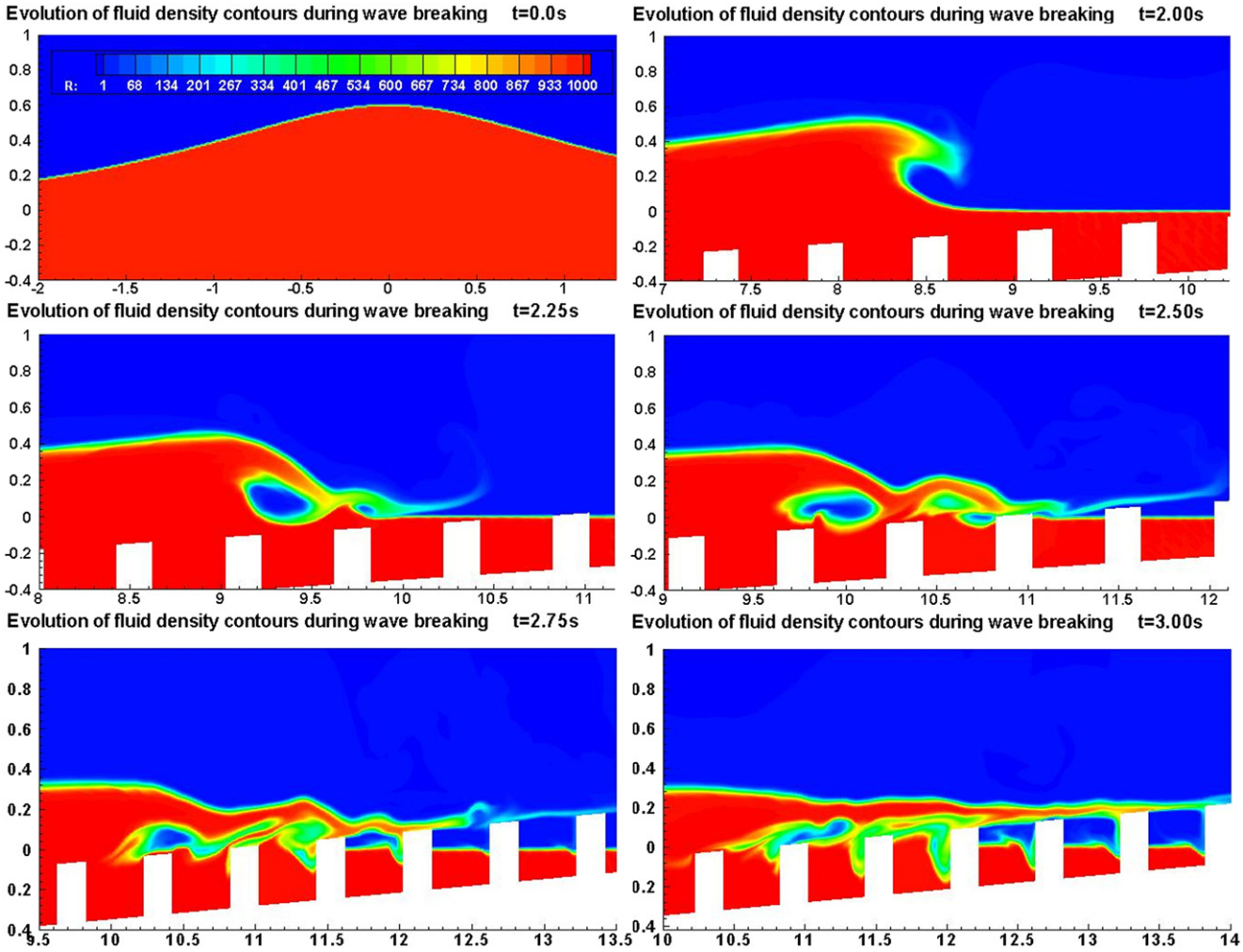

Fig. 11. Evolution of the fluid density contours during the solitary wave breaking process for case H03D04 at $t = 0$, 2, 2.25, 2.5, 2.75 and 3 s.

impaired by the presence of MR (cases *H02D08* and *H02D12*). The tendency to disturb the splash-up cycles, by either reinforcing or weakening the process depending on the location of the MR on the bottom slope, is enhanced by increasing D, e.g. in Fig. 8 for $t = 2.75$ s and $t = 3$ s. A closer view of vorticity fields in the vicinity of MR elements at $t = 2.75$ s for cases *H02D04* and *H02D12* is presented in Fig. 9. The effect of separation distance D on the vorticity fields is clearly identified. For a small D (left part of the figure), the MR elements are too close to allow the circulations induced by the form drag to penetrate and develop between them. An almost continuous sheared layer is formed on top of the MR and the effect on the main flow is nearly comparable to a reduction of the water depth. This in turn induces an earlier wave breaking compared to the flat sloping bottom case as shown in Fig. 8. For large separation distances, circulation cells develop in the wake of each MR element and affect the propagating wave all the way to the free surface. Let us now analyze the influence of the height H of the MR elements on breaking dynamics. Fig. 10 compares the free surface profile evolutions for cases *H00D00*, *H01D04*, *H02D04*, and *H03D04*. An observed tendency is steeper waves and earlier overturnings for an increasing H. On later stages, H is observed to play a preponderant role on the wave breaking. For sufficiently small roughness (case *H01D04* in Fig. 11), the splash-ups/rebounds cycles are not significantly affected by the presence of MR. Increasing H induces strong disturbances (case *H03D04* in Fig. 12) with encapsulation of air pockets between MR elements.

The effect of MR on the breaking process depends on the height and separation distance of the MR elements, with respect to the wave and the slope parameters. For a basic analysis, the effects of local slope, wave steepness, currents and wind are neglected. The breaking point is assumed to be reached when the wave amplitude A increases up to a given percentage of the local depth, as proposed by [32]. Note that for the strong plunging breakers studied here, it is expected that the critical value largely exceeds the commonly used value and is closer to 1. This simply indicates that at the breaking point, the wave amplitude and the local depth are related and can be used indifferently as the normalizing parameter for H and D. Keeping in mind that a much larger number of simulations should be performed to propose a comprehensive parametric study with a regime diagram, general trends on the influence of MR on the breaking of solitary waves can however be deduced from the present data. The soliton amplitude $A = 0.6$ m is used here as the normalizing parameter. The influence of the MR separation distance is then conditioned by the dimensionless ratio D/A. On one hand, for $D/A < 1$, no circulation cells develop between the MR elements and the effect on the main flow is nearly comparable to a reduction of water depth inducing an earlier wave breaking. One the other hand, when $D/A > 1$, circulation cells develop in the wake of each MR element affecting all the fluid column and disturbing the free surface. Furthermore, the successive cycles of impact/splash-ups/rebounds are strongly impaired, with ejection of water when the flow encounters MR elements, and the run up distance is expected to decrease. The influence of the macro-roughness height depends then on the dimensionless ratio H/A.

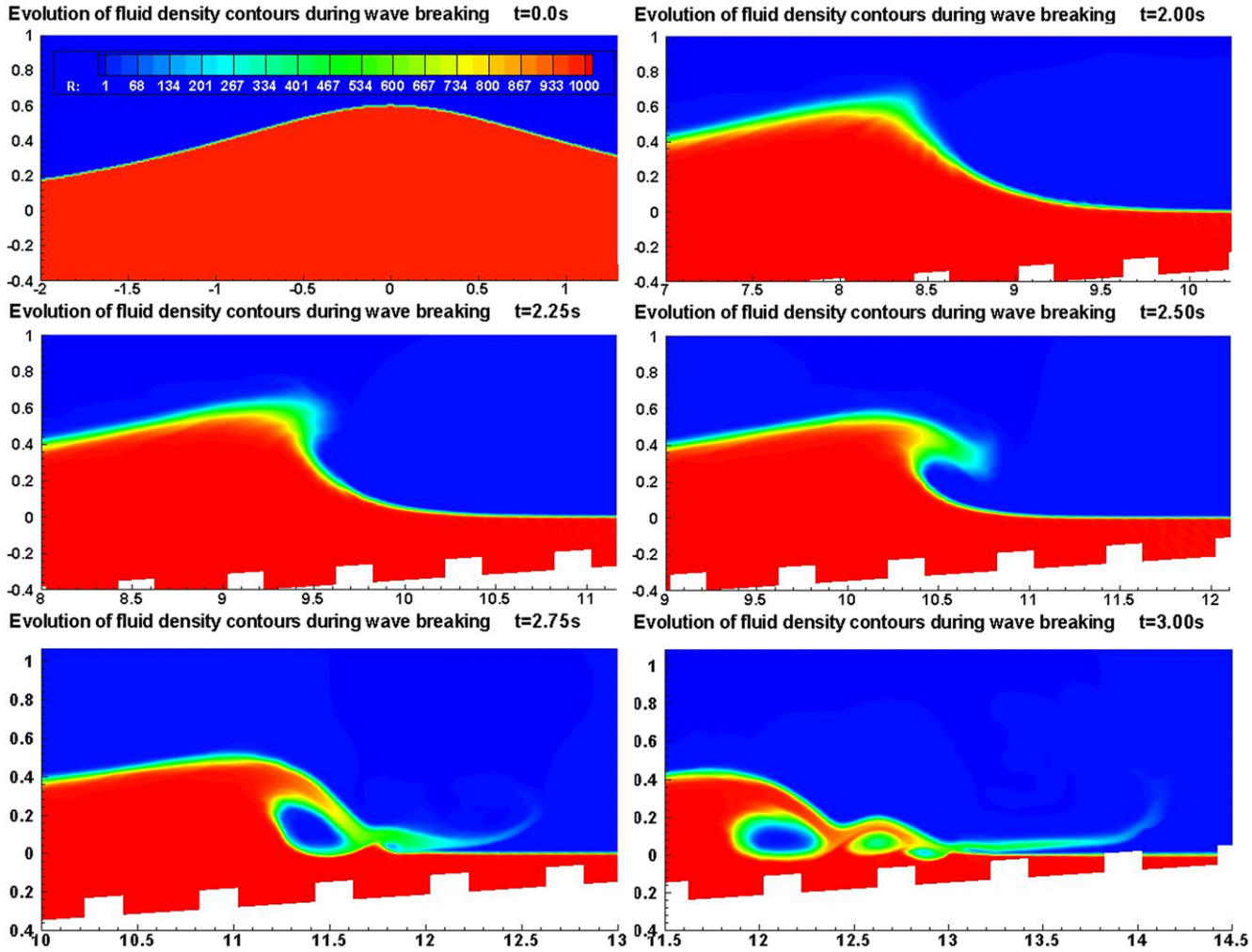

Fig. 12. Evolution of the fluid density contours during the solitary wave breaking process for case H01D04 at $t = 0$, 2, 2.25, 2.5, 2.75 and 3 s.

For $H/A < 0.25$, the only effect of MR is to induce earlier wave breaking. When $H/A > 0.25$, the overall breaking dynamics is modified, with strong disturbances of the splash-ups cycles and encapsulation of large air pockets between roughness elements.

The role played by the air entrapment on the wave breaking process is not obvious. However, interesting observations can be done by comparing the cases H03D04 and H01D04, shown in Figs. 11 and 12 respectively. For the small roughness case (H01D04) the fluid layer is too shallow and the MR are too small to allow entrapment of significant gas pockets between the MR elements. For sufficiently high MR (H03D04 case), air pockets generated by the splash-up/rebounds cycles can be trapped between the MR elements, as can be seen for $t = 2.75$ s and $t = 3$ s. The presence of such air pockets tends to prevent the jet rebounds. This can be observed by comparing the first splash-up cycle ($t = 2.25$ s and $t = 2.5$ s) for which the jet impacts and rebounds on pure water and the second cycle ($t = 2.5$ s and $t = 2.75$ s) for which the jet impacts nearly over a gas pocket and the rebound is inhibited. The sequence of impact/splash-up/rebound cycles is thus broken and the wave collapses, producing a kind of swash tongue sliding on the top of the MR elements (see Fig. 11 for $t = 3$ s).

3.5. 3D results

Fully three-dimensional solitary wave breaking over macro-roughness elements have been performed to assess the ability of the numerical model to simulate two phase flows over complex topography. The geometry is a 3D extension of the 2D case with a 0.5 m width. Symmetric conditions are imposed on the lateral boundaries. MR elements (height 0.2 m, length 0.2 m, width 0.1 m) regularly spaced by 0.8 m are located only on the lateral part of the bottom (see Fig. 13).

The 500 kg.m^{-3} isodensity surfaces evolution at $t = 2.625$, 3, 3.375, 3.75, 4.125 and 4.5 s is shown in Fig. 13. The shoaling process is only weakly affected by the presence of MR, i.e. no significant transverse destabilization is observed until $t = 2.625$ s. From $t = 3$ s, the overturning motion is accelerated over the bottom region covered by MR elements. After the jet impacts, the wave breaking becomes clearly three-dimensional. On one hand, the breaking over MR elements is quite similar to those observed in the previous 2D cases with successive splash-up cycles strongly affected by the obstacles and entrapment of air pockets. On the other hand, the flow over the smooth region of the bottom is faster and extends much further than over the rough region. It is also observed that on the upper part of the sloping bottom, the water penetrating between the MR elements first comes laterally from the rapid flow of the wave breaking over the smooth region, rather than from above. The overall wave front is no more uniform and horizontal vortical structures are formed.

For coastal protection concerns, it could be expected that a random MR distribution and height would generate a wide variety of vortical structures, both in size and direction. It should lead to stronger momentum transfers and therefore more dissipation of the wave energy. This hypothesis has obviously to be confirmed by further simulations.

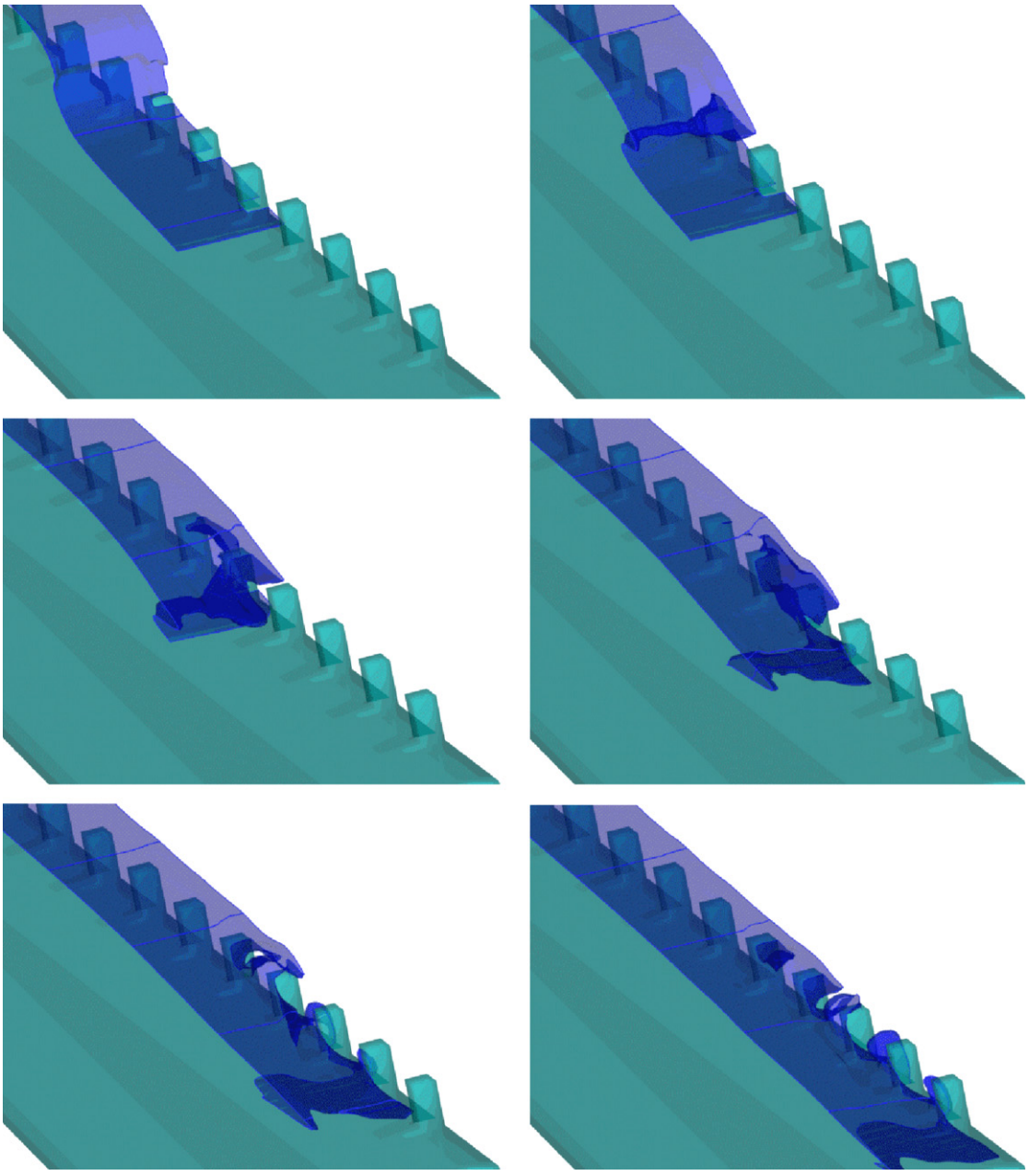

Fig. 13. Three-dimensional solitary wave breaking over macro-roughness elements. Sequence of 500 kg.m^3 isodensity surfaces at $t = 2.625$, 3, 3.375, 3.75, 4.125 and 4.5 s.

4. Conclusion

In this paper, numerical simulations of solitary wave breaking are performed solving Euler equations for a two phase flow model based on a hyperbolic system of conservation laws. In continuity of the work presented in [21], the physical aim of the study is to understand the influence of macro-roughness (MR) elements on the wave breaking dynamics. Viscosity and turbulence are not considered in the equations system restricting the applicability of the model to the early stages of breaking. However, the selected test cases are strong plunging breakers, in which the splash-up cycles take place in thin water layers or directly impact on the MR elements. It is thus expected that the breaking dynamics is dominated by impacts, pressure shocks and large coherent structures rather than by bottom friction or a well-established turbulent energy cascade.

This approach is validated by the satisfactory results obtained for the breaking on a sloping bottom with and without roughness elements. Generally observed features on flat sloping bottom, such as overturning motion, entrainment of air pockets, splash-up occurrence, dynamics generated by plunging breaking waves and generation of coherent vortex structures are well reproduced by the model. The influence of the MR elements on the solitary wave breaking is shown to depend on two dimensionless ratios D/A and H/A, where D, H and A are the separation distance between the MR elements, the height of the elements and the wave amplitude, respectively. Significant effects are observed for large values of D/A and H/A. The successive cycles of impact/splash-ups/rebounds are strongly impaired and the run up distance is expected to be reduced. Keeping in mind that a much larger number of simulations and comparisons with laboratory experiments and field measurements should be performed to propose a comprehensive parametric study for engineering purposes, the present results are expected to be useful to estimate the defensive potential of coastal structures. As an illustration of the efficiency of the numerical model in simulating complex wave-structure

interactions, a fully three-dimensional solitary wave breaking simulation over MR elements is presented.

The numerical prospects mainly concern interface compression and mesh refinement methods to improve the interface description. Further developments will also include the implementation of turbulent and viscous effects in order to describe the later stages of the breaking process and evaluate the run up height.

Acknowledgements

This work was granted by the TSUMOD project of the French Agence Nationale de la Recherche ANR-05-CATT-O16 and has been supported by the Region Provence Alpes Cote Azur. Computations were performed on the Regional PACA—Conseil General 83 SOCOM cluster. The authors would like to acknowledge the financial and scientific support of the INSU—CNRS program IDAO and the SHOM program PEA ECORS.

Prof. P. Helluy is warmly acknowledged for his help in the numerical code development and assessment.

References

[1] L. Hamm, P. Madsen, D. Peregrine, Wave transformation in the near-shore zone: a review, Coastal Eng. 21 (1993) 5–39.
[2] D. Peregrine, Breaking waves on beaches, Annu. Rev. Fluid Mech. 15 (1983) 149–178.
[3] E.D. Christensen, Large eddy simulation of spilling and plunging breakers, Coastal Eng. 53 (2006) 463–485.
[4] H. Fernando, S. Samarawickrama, S. Balasubramanian, S. Hettiarachchi, S. Voropayev, Effects of porous barriers such as coral reefs on coastal wave propagation, J. Hydro-eviron. Res. 1 (2008) 187–194.
[5] S. Grilli, J. Skourup, I. Svendsen, An efficient boundary element method for nonlinear water waves, Eng. Anal. Bound. Elem. 6 (2) (1989) 97–107.
[6] S. Grilli, P. Guyenne, F. Dias, A fully non-linear model for three-dimensional overturning waves over an arbitrary bottom, Internat. J. Numer. Methods Fluids 35 (2001) 829–867.
[7] P. Lin, P.L.F. Liu, A numerical study of breaking waves in the surf zone, J. Fluid Mech. 359 (1998) 239–264.
[8] S. Vincent, J. Caltagirone, P. Lubin, T. Randrianarivelo, An adaptive augmented Lagrangian method for three-dimensional multimaterial flows, Comput. & Fluids 33 (10) (2004) 1273–1289.
[9] S. Guignard, R. Marcer, V. Rey, C. Kharif, P. Fraunié, Solitary wave breaking on sloping beaches: 2-d two phase flow numerical simulation by sl-vof method, Eur. J. Mech. B Fluids 20 (1) (2001) 57–74.
[10] B. Biausser, S. Guignard, R. Marcer, P. Fraunié, 3D two phase flows numerical simulations by sl-vof method, Internat. J. Numer. Methods Fluids 45 (6) (2004) 581–604.
[11] B. Braconnier, J.J. Hu, Y.Y. Niu, B. Nkonga, K.M. Shyne, Numerical simulation of low mach compressible two-phase flows: preliminary assessments of some basic solution techniques, vol. 28, 2009, pp. 117–134.
[12] D. Fuster, G. Agbaglah, C. Josserand, S. Popinet, S. Zaleski, Numerical simulation of droplets, bubbles and waves: state of the art, Fluid Dyn. Res. 41 (6) (2009).
[13] A. Khayyer, H. Gotoh, Enhanced predictions of wave impact pressure by improved incompressible sph methods, Appl. Ocean Res. 31 (2) (2009) 111–131. S., S. S..
[14] T. Yasuda, H. Mutsuda, N. Mizutani, Kinematic of overturning solitary waves and their relations to breaker types, Coastal Eng. 29 (1997) 317–346.
[15] P. Helluy, F. Golay, J. Caltagirone, P. Lubin, S. Vincent, D. Drevrard, R. Marcer, P. Fraunié, N. Seguin, S. Grilli, A. Lesage, A. Dervieux, O. Allain, Numerical simulation of wave breaking, ESAIM: M2AN 39 (3) (2005) 591–607.
[16] F. Golay, P. Helluy, Numerical schemes for low mach wave breaking, Int. J. Comput. Fluid Dyn. 21 (2) (2007) 69–86.
[17] G. Chanteperdrix, P. Villedieu, J. Vila, A compressible model for separated two-phase flows computations, in: ASME, 2002.
[18] R. Saurel, R. Abgrall, A simple method for compressible multifluid flows, SIAM J. Sci. Comput. 21 (3) (1999) 1115–1145.
[19] K. Kleefsman, G. Fekken, A. Veldman, B. Iwanoski, B. Buchner, A volume-of-fluid based simulation method for wave impact problems, J. Comput. Phys. 206 (1) (2005) 363–393.
[20] F. Dias, D. Dutykh, J.M. Ghidaglia, A two-fluid model for violent aerated flows, Comput. & Fluids 31 (2) (2010) 283–293.
[21] A.N. Sambe, F. Golay, P. Fraunié, D. Sous, V. Rey, R. Marcer, C. DeJouette, Two phases flow unstructured grid solver: application to tsunami wave impact, in: ISOPE, 2009.
[22] S. Kokh, G. Allaire, Numerical simulation of 2d two-phase flows with interface, in: Godunov Methods: Theory and Applications, E. F. ToroKluwer Academic/Plenum, Dordrecht, New York, 2001.
[23] R. Plumerault, D. Astruc, M. Mory, P. Maron, P. Villedieu, Simulations de l impact de vagues sur une structure verticale prenant en compte la compressibilite du liquide, in: CFM, 2009.
[24] R. Abgrall, How to prevent pressure oscillations in multicomponent flow calculations: a quasi-conservative approach, J. Comput. Phys. 125 (1996) 150–160.
[25] G. Allaire, S. Clerc, S. Kokh, A five-equation model for the simulation of interfaces between compressible fluids, J. Comput. Phys. 181 (2002) 577–616.
[26] E. Godlewski, P.-A. Raviart, Numerical Approximation of Hyperbolic Systems of Conservation Laws, in: Applied Math. Sciences, vol. 118, Springer-Verlag, 1996.
[27] M. Tanaka, The stability of solitary waves, Phys. Fluids 29 (3) (1986) 650–655.
[28] Y. Li, F. Raichlen, Breaking criterion and characteristics for solitary waves on slopes, J. Waterw. Port Coastal Ocean Eng. 124 (6) (1998) 329–333.
[29] S. Grilli, I. Svendsen, R. Subramanya, Breaking criterion and characteristic for solitary waves on slopes, J. Waterw. Port Coastal Ocean Eng. 17 (6) (1997) 374–391.
[30] P. Lubin, S. Vincent, S. Abadie, J. Caltagirone, Three-dimensional large eddy simulation of air entrainment under plunging breaking waves, Coastal Eng. 53 (2006) 631–655.
[31] O. Kimmoun, H. Branger, A particle image velocimetry investigation on laboratory surf-zone breaking waves over a sloping beach, J. Fluid Mech. 588 (2007) 353–397.
[32] A. Seyama, A. Kimura, The measured properties of irregular wave breaking and wave height change after breaking on the slope, in: Proceedings of 21st International Conference on Coastal Engineering, 1998.